A Large Class of Chaotic Sensing Matrices for Compressed Sensing

Hongping Gan, Song Xiao, Yimin Zhao

PII: S0165-1684(18)30112-9
DOI: 10.1016/j.sigpro.2018.03.014
Reference: SIGPRO 6772

To appear in: *Signal Processing*

Received date: 28 November 2017
Revised date: 8 February 2018
Accepted date: 19 March 2018

Please cite this article as: Hongping Gan, Song Xiao, Yimin Zhao, A Large Class of Chaotic Sensing Matrices for Compressed Sensing, *Signal Processing* (2018), doi: 10.1016/j.sigpro.2018.03.014

Highlights

- A large class of chaotic sensing matrices is proposed based on topologically conjugate chaotic systems.
- A zone matching algorithm is elaborated for generating independently and identically distributed chaotic stream.
- Performance of the proposed sensing matrices is analyzed from the mutual coherence viewpoint.
- Performance of the proposed matrices is slightly better than the state-of-the-art sensing matrices.

A Large Class of Chaotic Sensing Matrices for Compressed Sensing

Hongping Gan, Song Xiao*, Yimin Zhao

State Key Lab of Integrated Services Networks
Xidian University, Xi'an, 710071, China

Abstract

Compressed sensing is a revolutionary sampling framework at a sub-Nyquist rate, which relies potentially on sensing matrix. In this paper, a large class of chaotic sensing matrices with low complexity, hardware-friendly implementation and desirable sampling efficiency is proposed based on topologically conjugate chaotic systems (TCcSs). Specifically, we first elaborate an independently and identically distributed chaotic stream, which is generated from a TCcS via our customized zone matching algorithm. Then, the chaotic stream is employed to construct the novel chaotic sensing matrix. Our framework encompasses various families of TCcSs for establishing sensing matrices, such as TCcSs of Tent chaotic system. Moreover, the mutual coherence of the proposed sensing matrices is investigated, and it shows that this kind of chaotic sensing matrices has similar sampling efficiency to that of the state-of-the-art sensing matrices. Experimental performances verify the correctness of the theoretical analysis and illustrate that the proposed matrices can provide comparable results against the existing ones.

Keywords: Sensing matrix, Topologically conjugate function, Chaotic stream, Mutual coherence

1. Introduction

Conventional techniques to sample and reconstruct a signal of interest are based on the principle of the Shannon-Nyquist's celebrated theory: the sampling rate is dictated by the bandwidth present in the signal [1]. Unluckily, due to the high sampling rate, this paradigm is subject to inefficiency and high consumption in case that the signal in some emerging applications exhibits (ultra-)high frequency. Compressed sensing (CS) initiated by Candès is an alternative theory that goes against the traditional wisdom in signal sampling procedure [2–4]. As opposed to traditional Shannon-Nyquist theorem, CS can recover the signal from far fewer samples than what is conventionally deemed requirement, and it has already attracted an increased interest at the intersection of statistics, mathematics, computer science, physics, electrical engineering, and biology [5–8].

In essence, CS provides a framework for sampling and compressing the original high-dimensional sparse signal $\boldsymbol{x_o} \in \boldsymbol{R}^N$ simultaneously. It depends on linear dimensionality reduction by using sensing matrix $\boldsymbol{M} \in \boldsymbol{R}^{M\times N}(M \ll N)$, i.e., the samples $\boldsymbol{y_o}$ are directly obtained by $\boldsymbol{y_o} = \boldsymbol{M}\cdot\boldsymbol{x_o} + \boldsymbol{\wp}$, where the ratio M/N denotes the sampling rate, $\boldsymbol{\wp}$ is noise, and the sparsity S of $\boldsymbol{x_o}$ is calculated by $||\boldsymbol{x_o}||_0 = \sum_{j=1}^{N}|x_j|^0$. In most cases, $\boldsymbol{x_o}$ is not sparse but compressible in some transform domain or a frame $\boldsymbol{\Psi} \in \boldsymbol{R}^{N\times N}$, that is, $\boldsymbol{x_o}$ can be transformed as coefficient vector $\boldsymbol{v}$ utilizing $\boldsymbol{\Psi}\cdot\boldsymbol{v}$ with $\boldsymbol{v}$ being S sparse. In these cases, the samples can be attained as:

$$\boldsymbol{y_o} = \boldsymbol{M}\cdot\boldsymbol{x_o} + \boldsymbol{\wp} = \boldsymbol{M}\cdot\boldsymbol{\Psi}\cdot\boldsymbol{v} + \boldsymbol{\wp}. \tag{1}$$

Note that Eq. (1) is highly underdetermined with $M \ll N$. If we elaborate a sensing matrix with some particular properties or characteristics that guarantee exact sampling performance, CS demonstrates that one can employ some efficient algorithms to reconstruct $\boldsymbol{x_o}$ from highly incomplete samples $\boldsymbol{y_o}$, for example, the l_0 algorithm

$$\boldsymbol{v}^* = argmin||\boldsymbol{v}||_{l_0} \quad subject \quad to \quad \boldsymbol{y_o} = \boldsymbol{M}\cdot\boldsymbol{\Psi}\cdot\boldsymbol{v} + \boldsymbol{\wp}.$$

By all accounts, one of key technologies of CS is to obtain a sensing matrix that satisfies the following requirements: 1) (near-)optimal sampling performance, and 2) universality, and 3) low complexity and fast reconstruction, and 4) hardware-friendly implementation [8]. Several properties have been proposed for evaluating the sampling performance of sensing matrices [9–11]. A well-known criterion called restricted isometry property (RIP) [9], developed by Candès from a geometric perspective, utilizes a restricted isometry constant (RIC) δ_S to set up the optimal sampling performance pledge at present. The δ_S is the smallest nonnegative number such that

$$\forall \boldsymbol{q} \in \boldsymbol{R}^{|S|}, \quad (1-\delta_S) \le \frac{\|\boldsymbol{M}_S\cdot\boldsymbol{q}\|_2^2}{\|\boldsymbol{q}\|_2^2} \le (1+\delta_S)$$

with a fixed sparsity S [10]. However, verifying the RIP of a sensing matrix is an NP-Hard problem, since one needs to compute all the RICs of the sub-matrices with S columns selected from $\boldsymbol{M}$.

Mutual coherence [11] is a practical evaluation criterion to ensure the sampling quality of sensing matrices. Mathematically, the mutual coherence is quantified by

$$u(\boldsymbol{M}) = \max_{1\le i\ne j\le N} \frac{\|\boldsymbol{m_i}^T\cdot\boldsymbol{m_j}\|}{||\boldsymbol{m_i}||_2\cdot||\boldsymbol{m_j}||_2}, \tag{2}$$

*Corresponding author:Song Xiao
Email addresses: ganhong112@163.com (Hongping Gan), xiaosong1xidian@sina.com (Song Xiao)

where $\boldsymbol{m_i}$, $\boldsymbol{m_j}$ are the i^{th} and j^{th} columns of $\boldsymbol{M}$, respectively, the $(\cdot)^T$ means transposition operator. Note that the mutual coherence $u(\boldsymbol{M})$ is limited in the interval $[\sqrt{\frac{N-M}{M(N-1)}}, 1]$, where $\sqrt{\frac{N-M}{M(N-1)}}$ is the optimal bound [12]. By using the coherence, one can more easily check and investigate the sampling performance of sensing matrices in contrast with RIP. Hence, the mutual coherence has been broadly applied to measure the capability of sensing matrices [13].

Up to date, many types of sensing matrices [14–18] have been presented for CS literature according to the guideline of the mutual coherence or the RIP. The existing well-designed sensing matrices can be classified into two categories in terms of their inner elements: random sensing matrices and deterministic sensing matrices. Random matrices, possibly the most famous sensing matrices, have been certified to yield favorable mutual coherence [14]. A crucial advantage of random sensing matrices is universality that $\boldsymbol{M} \cdot \boldsymbol{\Psi}$ will be uncorrelated with overwhelming probability regardless of the choice of $\boldsymbol{\Psi}$, provided that $M \geq \mathcal{O}(S \cdot \log(N/S))$ [8]. Nonetheless, random matrices naturally have three major shortcomings in applications: 1) low storage efficiency, and 2) high computational complexity, and 3) difficult to design in hardware [15]. In order to overcome the drawbacks of the random matrices, another class of sensing matrices, for example, Hadamard-Walsh matrix [16] or Binary sensing matrix [17], has been proposed and used for particular applications [18]. Unfortunately, due to loss of randomness, deterministic sensing matrices only perform well with $\boldsymbol{\Psi} = \boldsymbol{I}$, which greatly hinders the possible range of its applications.

Consequently, to combine the merits of both random constructions and deterministic ones, many researchers have investigated a popular chaotic family of sensing matrices in succession. In an early attempt, Yu *et al.* have shown that Logistic chaotic matrix, generated by Logistic chaotic sequence, satisfies RIP with very high probability, which guarantees the sampling performance [19]. Similarly, Frunzete *et al.* have established Tent chaotic sensing matrix, which exhibits very close sampling quality to that of random sensing matrices [20, 21]. Kafedziski *et al.* have presented that Chua or Lorenz chaotic sequence can be suitable to construct chaotic sensing matrix [22]. Meanwhile, Gan *et al.* have indicated that Chebyshev chaotic sensing matrix is an alternative to such above chaotic matrices, which can directly overcome the useless transient iterations [23]. Moreover, Zeng *et al.* have introduced a structural chaotic matrix and proved that this kind of matrix yields low mutual coherence [24, 25]. Magically, the chaotic CS-based framework can provide desirable virtue that encryption occurs implicitly at the sampling procedure [26, 27]. Therefore, the applications of chaotic compressed sensing have attracted a great deal of researchers' attention in various fields, such as image [28–30], healthcare monitoring system [31, 32], and wireless sensor network [33–35].

Although the aforementioned chaotic sensing matrices exhibit an encouraging performance, the drawbacks of chaotic systems would enormously limit their practical applications. Due to the limited precision of electronic devices, the chaotic sequences may quickly converge to zero, resulting in that chaotic systems meet the degradation phenomenon [36–38], which may further significantly enlarge the mutual coherence of chaotic sensing matrices. Division, multiplication, (non-)linear operation, sine and cosine triangular calculations of real numbers may trigger errors by quantization, rounding or overflowing, which may lead to a great difference between actual chaotic orbit and theoretical one [37]. Several works have been done to alleviate the degradation problem of some one-dimensional chaotic systems, for example, piecewise linear chaotic system [36] and Logistic chaotic system [38]. However, it can not fundamentally counteract the degradation problem incurred by the limited precision effects.

It is well-known that the topologically conjugate chaotic system (TCcS) consists of two transformations and a continuous and invertible function. In particular, TCcS can be easily designed by feedback control in hardware implementation [39, 40]. One of the most attractive characteristics of TCcS is that TCcS can generate an infinite, and independently and identically distributed (i.i.d) chaotic stream, which can avoid the degradation phenomenon [41, 42]. TCcS plays an important role in the information field, which has inspired numerous researches, such as cryptography [41] and digital communication systems [42].

In this paper, we establish the chaotic sensing matrix by utilizing the i.i.d chaotic stream generated by the TCcS. Note that we take advantage of an i.i.d chaotic stream rather than directly utilize a chaotic sequence to build the chaotic sensing matrix. Specially, a zone matching algorithm is derived for generating the i.i.d chaotic stream from a TCcS of Tent chaotic system. The proposed algorithm first divides one of the two transformations of the TCcS to many sub-zones according to the continuous and invertible function. Then, by matching sub-zone rather than adopting real value of an iteration, the proposed algorithm can generate an infinite and i.i.d chaotic stream, which overcomes the degradation phenomenon incurred by the limited precision effects.

Such an algorithm can be applied to other TCcSs [43, 44], such as TCcSs of Lorenz chaotic system [44]. Therefore, we further establish one large class of chaotic sensing matrices from multiple choices of the TCcSs. Moreover, we analyze the mutual coherence of the proposed sensing matrices and show that this kind of chaotic sensing matrices has similar sampling efficiency to that of the state-of-the-art sensing matrices. Extensive numerical results verify the correctness of the theoretical analysis and illustrate that the proposed sensing matrices can provide comparable performances against typical sensing matrices. Meanwhile, thanks to the characteristics of TCcSs, the proposed chaotic matrices have low complexity, can facilitate the hardware implementation, and would be more propitious in particular applications that claim privacy and security.

The rest of this paper is outlined as follows. Our main results are presented in Sect. 2 and Sect. 3. Sect. 2 illustrates how to generate an i.i.d stream from a TCcS via our zone matching algorithm. The proposed chaotic matrices are constructed, and analyzed from the mutual coherence aspect in Sect. 3. Sect. 4

gives numerical validations with sparse signal and real image to illustrate the comparability of the proposed sensing matrices to the existing ones. The conclusions are presented in Sect. 5.

2. Generation of i.i.d stream from TCcS via zone matching algorithm

In this section, we present how to generate an i.i.d stream from a TCcS via our customized zone matching algorithm. In order to verify the zone matching algorithm can indeed produce the i.i.d stream, we first obtain a chaotic stream from a TCcS via our customized algorithm, then we prove that the chaotic stream is i.i.d from a statistical standpoint.

2.1. Topologically conjugate function

Definition 1 (Topologically conjugate function [42, 45]). For two functions, $U(\cdot) : \mathrm{H} \to \mathrm{H}$, with probability density ρ_u; $W(\cdot) : \mathrm{L} \to \mathrm{L}$, with probability density ρ_w,

$$\begin{aligned} z_{k+1} &= U(z_k) \qquad (z \in \mathrm{H} = [-|c|, |c|]), \\ t_{k+1} &= W(t_k) \qquad (t \in \mathrm{L}), \end{aligned}$$

where $k \in \mathbb{N}$, if there has a continuous and invertible function $F(\cdot) := \{t_k = F(z_k) | \mathrm{H} \to \mathrm{L}\}$ [1], such that

$$F^{-1} \circ U \circ F(z_k) = W(z_k),$$

where $U \circ F(z_k) \equiv U(F(z_k))$, then $U(\cdot)$ and $W(\cdot)$ are a pair of topologically conjugate functions via $F(\cdot)$.

Suppose $U(\cdot)$ and $W(\cdot)$ are topologically conjugated via $F(\cdot)$, one can easily derive the relation between two probability density functions ρ_u and ρ_w.

Lemma 1 (Relation between two probability density functions [42, 45])**.** *If we have a pair of topologically conjugate functions $U(\cdot)$ and $W(\cdot)$ via $F(\cdot)$, then the probability density function ρ_u of $U(\cdot)$ can be calculated by*

$$\rho_u(z) = \rho_w(F^{-1}(z)) \mid \frac{dF^{-1}(z)}{dz} \mid, \tag{3}$$

where ρ_w is the probability density function of $W(\cdot)$.

Eq. (3) can be verified from a simplified computation that the equidistributivity property is invariant under the topologically conjugate function [42].

There are numerous topologically conjugate chaotic systems in practical physics. Here, we only give two cases of TCcSs of Tent chaotic system.

Case 1: For Tent chaotic system,

$$W_1(z) = \begin{cases} 2z & 0 \le z \le 1/2 \\ 2 - 2z & 1/2 \le z \le 1, \end{cases} \tag{4}$$

when $h_1 c_1 = -2$,

$$U_1(z) = h_1 z^2 + c_1 \qquad (z \in [-|c_1|, |c_1|]),$$

$U_1(z)$ is topologically conjugated with $W_1(z)$ through $F_1(z) = -c_1 \cos(\pi z)$.

[1] Mathematically, function $F(\cdot)$ is what we term a 'homeomorphism'.

Proof. According to the definition of the topologically conjugate function, we want to get

$$F^{-1} \circ U \circ F(z_k) = W(z_k),$$

as long as we have

$$U \circ F(z_k) = F \circ W(z_k).$$

For system defined by Eq. (4) and $F_1(z) = -c_1 \cos(\pi z)$, if $h_1 c_1 = -2$, we can obtain

$$\begin{aligned} U_1 \circ F_1(z) &= -\frac{2}{c_1} \cdot {c_1}^2 \cos^2 \pi z + c_1 \\ &= -c_1 [2\cos^2(\pi z) - 1] \\ &= -c_1 \cos(2\pi z). \end{aligned}$$

Moreover,

$$\begin{aligned} F_1 \circ W_1(z) &= \begin{cases} -c_1 \cos(2\pi z) & 0 \le z \le 1/2 \\ -c_1 cos[\pi(2 - 2z)] & 1/2 \le z \le 1 \end{cases} \\ &= -c_1 \cos(2\pi z) \qquad 0 \le z \le 1. \end{aligned}$$

Obviously, $U_1 \circ F_1(z) = F_1 \circ W_1(z)$, i.e., $U_1(z)$ and $W_1(z)$ are topologically conjugated through $F_1(z)$. □

Case 1 provides extensive research spaces for searching topologically conjugate chaotic systems.

Example 1: taking $h_1 = -2$, $c_1 = 1$, we have

$$\begin{aligned} U_1(z) &= 1 - 2z^2 \qquad (z \in [-1, 1]), \\ F_1(z) &= -\cos(\pi z) \qquad (z \in [0, 1]). \end{aligned}$$

In example 1, $U_1(z)$ is the famous Logistic chaotic system. Similar to example 1, we can obtain

Example 2:

$$\begin{aligned} U_1(z) &= -4/5z^2 + 5/2, \\ F_1(z) &= -5/2\cos(\pi z), \end{aligned}$$

with $h_1 = -4/5$, $c_1 = 5/2$.

Case 2: For chaotic system described by Eq. (4), i.e.,

$$W_2(z) = W_1(z),$$

when $h_2 c_2 = -4$,

$$U_2(z) = h_2 z^2 + 4z \qquad (z \in [-|c_2|, |c_2|]),$$

$U_2(z)$ is topologically conjugated with $W_2(z)$ via

$$F_2(z) = -c_2 \frac{\sin^2(\pi z)}{2}.$$

Readers can prove case 2 in the same way as case 1 and derive some examples from case 2.

2.2. Theorem for generation of i.i.d stream

There have existed multiple analogous cases to find topologically conjugate functions [43, 44]. Because of the limitation of length, we only show two cases, and no more tautology. Owing to the properties of the TCcS, we can obtain the following theorem.

Theorem 1 (Theorem for generation of i.i.d stream)**.** *For the systems $U(z)$ and $F(z)$ defined by definition 1, if we choose d $(2 \le d \in \mathbb{N})$ as the sampling step, resulting in $z_{k+1} = U^d(z_k)$, $k \in \mathbb{N}$, then one can obtain an independently uniformly distributed chaotic stream $\{r_k\}_1^\infty$ via the zone matching algorithm (see algorithm 1).*

Algorithm 1 The zone matching algorithm for generating the i.i.d stream from TCcS

Require: The systems $U(z)$ and $F(z)$ defined by definition 1, an initial seed z_1, and a sampling step $d(2 \le d \in \mathbb{N})$;

Ensure: An i.i.d chaotic stream $\{r_k\}_1^\infty$;

Step I allocating sub-zones step:

Situation 1: if $c > 0$, we divide the chaotic attractor domain $[0, c]$ into $P = 2^d$ sub-zones $\tau_i = [b_i, b_{i+1})$, where $b_i = F(\frac{i}{P})$, $i = 1, 2, 3, \ldots, P$.

Situation 2: if $c < 0$, we divide the chaotic attractor domain $[c, 0]$ into $P = 2^d$ sub-zones $\tau_i = [b_i, b_{i+1})$, where $b_i = F(\frac{P-i}{P})$, $i = 1, 2, 3, \ldots, P$.

Step II matching sub-zones step:

By utilizing the value of z_k $(k \in \mathbb{N})$ to match sub-zones, one can obtain a primal chaotic stream $\{g_k\}_1^\infty$. Provided that $z_k \in \tau_i$, set the entry of primal chaotic stream $g_k = i$, and calculate $z_{k+1} = U^d(z_k)$.

Step III adjusting step:

Define the final chaotic stream $\{r_k\}_1^\infty$, where the element $r_k = \frac{g_k}{P} - \frac{1+P}{2P}$.

return $\{r_k\}_1^\infty$;

The zone matching algorithm goes through three stages: allocating sub-zones step, matching sub-zones step and adjusting step. The allocating sub-zones step first divides the chaotic attractor domain $U(z)$ to many sub-zones according to the homeomorphism $F(z)$. Then, by matching sub-zones, the proposed algorithm can generate a primal chaotic stream $\{g_k\}_1^\infty$. Finally, the stream $\{g_k\}_1^\infty$ is adjusted as $\{r_k\}_1^\infty$ with mean zero in the last step. Note that the zone matching algorithm utilizes the sub-zone match instead of the real value of an iteration to yield a stream, which can counteract the degradation problem.

Obviously, g_k has similar statistical characteristics to r_k because of the linear conversion. For example, if g_k and g_{k+1} are statistically independent, r_k and r_{k+1} would be statistically independent as well. Next, we show the validity of the theorem 1 by proving that case 1 can generate an i.i.d stream, as case 1 is a typical case of TCcSs.

Proof. Part A: $U_1(z)$ is surjective and chaotic. If $z_k \in [-|c_1|, |c_1|]$, one can easily conclude that

$$U_1(z_k) \in \begin{cases} H_1 = [0, c_1] & for \quad c_1 > 0 \\ H_2 = [c_1, 0] & for \quad c_1 < 0. \end{cases}$$

Hence, $U_1(z)$ is surjective in the field of definition. It's well-known that a pair of topologically conjugate functions have the same Lyapunov exponent [42–44]. Since the Lyapunov exponent of Tent chaotic system defined by Eq. (4) is equal to $\log 2$, the system $U_1(\cdot)$'s Lyapunov exponent is $\log 2 > 0$, which indicates that $U_1(\cdot)$ is chaotic.

Part B: The chaotic stream $\{g_k\}_1^\infty$ is uniformly distributed. By the topologically conjugate lemma, we obtain

$$\rho_u(z) = \rho_w(F^{-1}(z)) \mid \frac{dF^{-1}(z)}{dz} \mid .$$

Note that $\rho_{w_1}(\cdot) = 1$ [20], hence, the probability of $z_k \in \tau_i = [b_i, b_{i+1})$ is equal to

$$\begin{aligned} \int_{b_i}^{b_{i+1}} \frac{dF_1^{-1}(z)}{dz} &= \int_{F_1(\frac{i}{P})}^{F_1(\frac{i+1}{P})} dF_1^{-1}(z) = F_1^{-1}(z)\Big|_{F_1(\frac{i}{P})}^{F_1(\frac{i+1}{P})} \\ &= F_1^{-1}(F_1(\frac{i+1}{P})) - F_1^{-1}(F_1(\frac{i}{P})) \\ &= \frac{i+1}{P} - \frac{i}{P} = \frac{1}{P}. \end{aligned}$$

Therefore, the probability of z_k in each sub-zone is the same, i.e., the chaotic stream $\{g_k\}_1^\infty$ is uniformly distributed.

Part C: $\{g_k\}_1^\infty$ is statistically independent. Assume that $c_1 > 0$, one can easily derive that $z_k = F_1(\alpha) = c_1 \cos(\pi\alpha)$ is an even, one-to-one, increasing and periodic $T = 2$ function with $\alpha \in [0, 1]$. And $z_k \in \tau_i^j \Leftrightarrow \alpha \in [\frac{1}{P}(i + \frac{j}{P}), \frac{1}{P}(i + \frac{j+1}{P})]$, where the $\tau_i^j = [b_i^j, b_{i+1}^j)$, $j \in \{1, 2, \ldots, P\}$, $b_i^j = F_1(\frac{1}{P}(i + \frac{j}{P}))$. Consequently,

$$\begin{aligned} z_{k+1} &= U_1^d(z_k) = U_1^d(F(\alpha)) = U_1^{d-1}(F_1(2^1\alpha)) \\ &= U_1^{d-2}(F_1(2^2\alpha)) = \cdots = F_1(2^d\alpha) \\ &\in [F_1(\frac{2^d}{P}(i + \frac{j}{P})), F_1(\frac{2^d}{P}(i + \frac{j+1}{P}))] \\ &= [F_1(i + \frac{j}{P}), F_1(i + \frac{j+1}{P})] \\ &= \begin{cases} \left[F_1(\frac{j}{P}), F_1(\frac{j+1}{P})\right] & for\ i = 2D \\ \left[F_1(\frac{j+1-P}{P}), F_1(\frac{j-P}{P})\right] & for\ i = 2D+1, \end{cases} \end{aligned}$$

where $D = 0, 1, 2, \ldots$. Hence, according to the zone matching algorithm, when $g_k = i$,

$$g_{k+1} = \begin{cases} j & for \quad i = 2D \\ P - j - 1 & for \quad i = 2D+1. \end{cases} \tag{5}$$

Eq. (5) certificates that

$$Pro(g_k = i, g_{k+1} = j) = Pro(g_k = i) \cdot Pro(g_{k+1} = j). \tag{6}$$

More generally, due to the algorithm 1, Eq. (6) can be generalized as following:

$$\begin{aligned} &Pro(g_k = i, g_{k+1} = j, g_{k+2} = s, \cdots) = \\ &Pro(g_k = i) \cdot Pro(g_{k+1} = j) \cdot Pro(g_{k+2} = s) \cdots, \end{aligned} \tag{7}$$

where $i, j, s \in \{1, 2, 3, \ldots, P\}$, respectively. Eq. (7) implies that $\{g_k\}_1^\infty$ is statistically independent. Similar proving process can be applied to $c_1 < 0$, which is not repeated here.

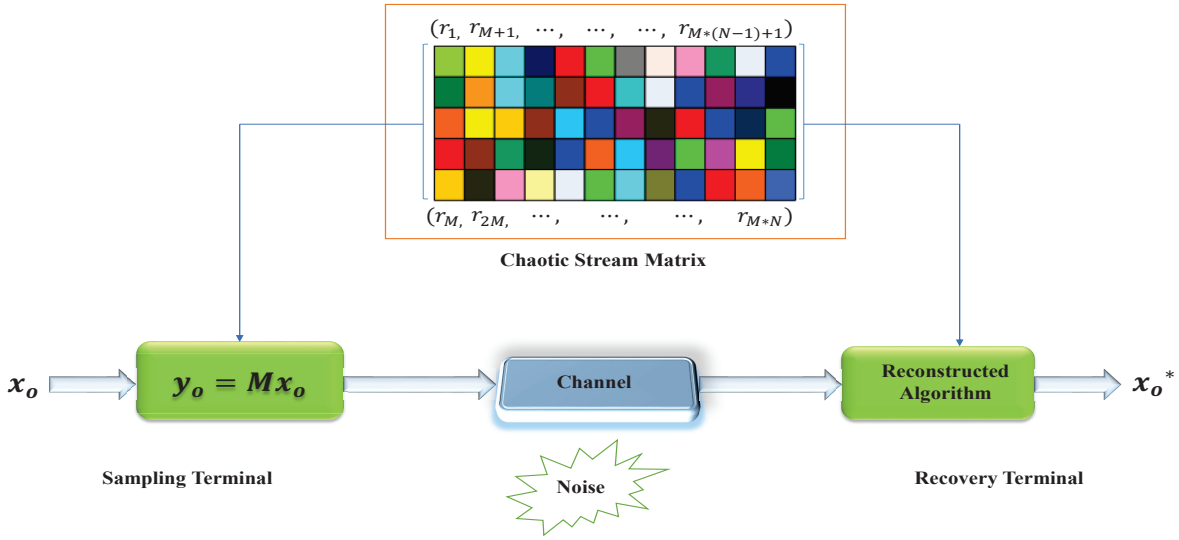

Figure 1: Diagrammatic drawing of CS with a chaotic stream sensing matrix.

By virtue of part A, B and C, it verifies that $\{g_k\}_1^\infty$ is statistically independently and identically distributed, leading to $\{r_k\}_1^\infty$ is also i.i.d, which completes the proof. □

The proof of theorem 1 with regard to other cases of TCcSs is analogous as above analysis.

2.3. Statistical characteristics of the chaotic stream

On the basis of the previous work, one can easily calculate the statistical characteristics of any chaotic stream $\{r_k\}_1^\infty$ generated by theorem 1.

As we know, the chaotic stream $\{g_k\}_1^\infty$ is uniformly distributed, which results in that $\{r_k\}_1^\infty$ has the following properties: zero mean, uniformly distributed, values bounded within the interval $[-\frac{1}{2}+\frac{1}{2P}, \frac{1}{2}-\frac{1}{2P}]$. Approximately, if the sampling distance d of the algorithm 1 is chosen large enough, leading to that $P = 2^d \to \infty$, one can get that $\{r_k\}_1^\infty$ subjects to $\mathscr{U}(-\frac{1}{2}+\frac{1}{2P}, \frac{1}{2}-\frac{1}{2P})$. Thus, we can compute the expectation of $\{r_k\}_1^\infty$, i.e.,

$$E(r) = \frac{(-\frac{1}{2}+\frac{1}{2P})+(\frac{1}{2}-\frac{1}{2P})}{2} = 0.$$

And the variance σ_r^2 of $\{r_k\}_1^\infty$ is equal to

$$\sigma_r^2 = \frac{[(\frac{1}{2}-\frac{1}{2P})-(-\frac{1}{2}+\frac{1}{2P})]^2}{12} = \frac{(1-\frac{1}{4P})^2}{12} \to \frac{1}{12}.$$

Remark 1: The i.i.d chaotic stream $\{r_k\}_1^\infty$ generated by our customized algorithm can avoid the degradation phenomenon that the chaotic sequence may quickly converge to zero. This advantage of the chaotic steam would be particularly favorable for constructing a sensing matrix.

Remark 2: Note that theorem 1 doesn't specify a specific chaotic system, i.e., besides topologically conjugate systems of Tent chaotic system, there are many other TCcSs, such as TCcSs of Lorenz chaotic system, which can be also used to generate an i.i.d stream via the zone matching algorithm. Consequently, we can establish one large class of chaotic sensing matrices from multiple choices of the TCcSs.

Remark 3: The initial seed z_1 and the sampling distance d of the TCcS determine the chaotic stream $\{r_k\}_1^\infty$ according to the customized algorithm. A different z_1 or d will generate an entirely different chaotic stream, which further results in a different chaotic sensing matrix. Therefore, z_1 and d can be considered as a secret key to build the sensing matrix, which would be more favorable in CS applications.

3. Chaotic stream sensing matrices and its benefits

This section shows how to build a sensing matrix for CS literature based on a chaotic stream $\{r_k\}_1^\infty$. Moreover, we investigate the mutual coherence and the benefits of the proposed sensing matrices against typical sensing matrices.

3.1. Construction of chaotic stream sensing matrices

In a similar way to generate typical sensing matrices, we can fill the entries of sensing matrix $\boldsymbol{M}$ by the chaotic steam $\{r_k\}_1^\infty$ with length $M \times N$, that is

$$\boldsymbol{M}_{CSM} = \frac{1}{\sigma_r\sqrt{M}} \begin{pmatrix} r_1 & r_{(M+1)} & r_{(2M+1)} & \cdots & r_{M\times(N-1)+1} \\ r_2 & r_{(M+2)} & r_{(2M+2)} & \cdots & r_{M\times(N-1)+2} \\ r_3 & r_{(M+3)} & r_{(2M+3)} & \cdots & r_{M\times(N-1)+3} \\ \vdots & \vdots & \vdots & \ddots & \vdots \\ r_M & r_{(2M)} & r_{(3M)} & \cdots & r_{M\times N} \end{pmatrix}, \tag{8}$$

where the factor $\frac{1}{\sigma_r\sqrt{M}}$ is for standardization. Obviously, the elements of M_{ij} are selected from $\{r_k\}_1^\infty$ in one reasonable queue.

The CS literature with a chaotic stream sensing matrix (CSM) can be illustrated as Fig. 1. At the sampling terminal, one can sample and compress the original signal $\boldsymbol{x_o}$ within one-step due to the CSM with $M << N$. In practical applications, there always exists noise because of the quantization or the transmission. At the recovery terminal, recovery algorithms like l_0 algorithm can be utilized to reconstruct $\boldsymbol{x_o}$. In order to verify the proposed matrices can indeed ensure the sampling performance for CS, we investigate the mutual coherence of the proposed sensing matrices in the next subsection.

3.2. Mutual Coherence of CSM

As we know, the entries M_{ij} of the CSM are i.i.d, hence, the columns of $\boldsymbol{M}$ can be viewed as i.i.d random vectors with deterministic elements. There have existed some research achievements to support that i.i.d random matrices yield low mutual coherence [11–15]. Next, we report an interesting theorem for the proposed sensing matrices from mutual coherence viewpoint. To begin with, let recall joint correlation lemma.

Lemma 2 (Joint correlation lemma)**.** *Consider $\{\boldsymbol{c_i}\}$ be a series of S vectors with $||\boldsymbol{c_i}||_2 \leq 1$, and $\boldsymbol{\theta}$ is a random vector whose elements are independently drawn from a certain distribution with mean zero and variance $\frac{1}{M}$, such as $\mathcal{N}(0,\frac{1}{M})$. Provided that $\boldsymbol{c_i}$ is independent of $\boldsymbol{\theta}$, we obtain*

$$Pro(\max_i |<\boldsymbol{\theta},\boldsymbol{c_i}>| \leq \beta) \geq 1 - S\exp(\frac{M\beta^2}{2}). \tag{9}$$

Proof. Obviously, the probability of Eq. (9) only depends on the size of $\boldsymbol{c_i}$. Hence, we can suppose that the certain distribution is a normal distribution $\mathcal{N}(0,\frac{1}{M})$ and each $||\{\boldsymbol{c_i}\}||_2$ is equal to 1. Because $\boldsymbol{\theta}$ is a random vector whose elements are independently drawn from distribution $\mathcal{N}(0,\frac{1}{M})$, it leads to that $<\boldsymbol{\theta},\boldsymbol{c_i}>$ obeys the distribution $\mathcal{N}(0,\frac{1}{M})$ as well. According to the Gaussian tail bound, we have

$$\begin{aligned} Pro(|<\boldsymbol{\theta},\boldsymbol{c_i}>| > \beta) &= \sqrt{\frac{2}{\pi}}\int_{\beta\sqrt{M}}^{+\infty} e^{-\frac{w^2}{2}}dw \\ &\leq \exp(-\frac{M\beta^2}{2}). \end{aligned}$$

By combining with the Boole's inequality, we obtain

$$Pro(\max_i |<\boldsymbol{\theta},\boldsymbol{c_i}>| \leq \beta) \geq 1 - S\exp(-\frac{M\beta^2}{2}),$$

which finishes the proof. □

By observing coherence analysis of random sensing matrices with joint correlation lemma, one can obtain the following theorem.

Theorem 2 (Theorem for mutual coherence of CSM)**.** *The mutual coherence of CSM with the form of Eq. (8) is equal to $\sqrt{\frac{c_3\log(N/\gamma)}{M}}$ with the probability $Pro > 1-\gamma^2$, where $\gamma \in (0,1)$ and c_3 is a constant.*

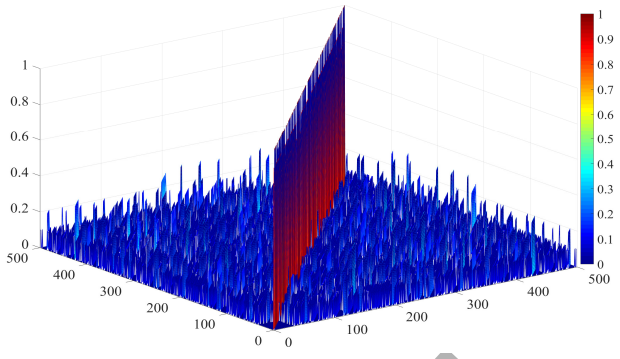

Figure 2: The entries of $\boldsymbol{G} \in \boldsymbol{R}^{500\times500}$ with respect to CSM with sizes 300×500.

Proof. As shown in Eq. (8), the column of CSM is normalized by scalar $\frac{1}{\sigma_r\sqrt{M}}$, therefore, we can define

$$Q_t = \frac{\|\boldsymbol{m_i}^T\cdot\boldsymbol{m_j}\|}{||\boldsymbol{m_i}||_2\cdot||\boldsymbol{m_j}||_2} = \|\boldsymbol{m_i}^T\cdot\boldsymbol{m_j}\| = <\boldsymbol{m_i},\boldsymbol{m_j}>,$$

where $t = 1,2,\ldots,N$.

Because $\boldsymbol{m_i}$ and $\boldsymbol{m_j}$ are i.i.d random vectors whose elements are independently extracted from the distribution $\mathscr{U}[(-\frac{1}{2}+\frac{1}{2P})/(\sigma_r\sqrt{M}),(\frac{1}{2}-\frac{1}{2P})/(\sigma_r\sqrt{M})]$ with mean zero and variance $\frac{1}{M\sigma_r^2}$, $\boldsymbol{m_i}$ and $\boldsymbol{m_j}$ are mutually independent. According to lemma 2, we get

$$\begin{aligned} &Pro(\max_{1\leq i\neq j<N} |<\boldsymbol{m_i},\boldsymbol{m_j}>| > \beta) \\ &\leq \frac{1}{2}N(N-1)\exp(-\frac{M\sigma_r^2\beta^2}{2}). \end{aligned}$$

Let define $Q = \{\max_{1\leq i\neq j<N}|<\boldsymbol{m_i},\boldsymbol{m_j}>|\}$, we have

$$\begin{aligned} Pro(Q>\beta) &\leq \frac{1}{2}N(N-1)\exp(-\frac{M\sigma_r^2\beta^2}{2}) \\ &< N^2\exp(-\frac{M\sigma_r^2\beta^2}{2}). \end{aligned} \tag{10}$$

We can substitute the Eq. (10) by $\beta = \sqrt{\frac{4\log(\frac{N}{\gamma})}{M\sigma_r^2}}$ $(0<\gamma<1)$, which leads to that

$$\begin{aligned} Pro(Q > \sqrt{\frac{4\log(\frac{N}{\gamma})}{M\sigma_r^2}}) &< N^2\exp(-2\log(\frac{N}{\gamma}) \\ &= \gamma^2. \end{aligned}$$

Together with the Boole's inequality, we obtain

$$Pro(Q \leq \sqrt{\frac{4\log(\frac{N}{\gamma})}{M\sigma_r^2}}) > 1-\gamma^2.$$

By virtue of the definition of Eq. (2), we can obtain the mutual coherence of CSM, i.e.,

$$u_{CSM} = \sqrt{\frac{c_3\log(\frac{N}{\gamma})}{M}}.$$

where c_3 is a constant. This ends the proof. □

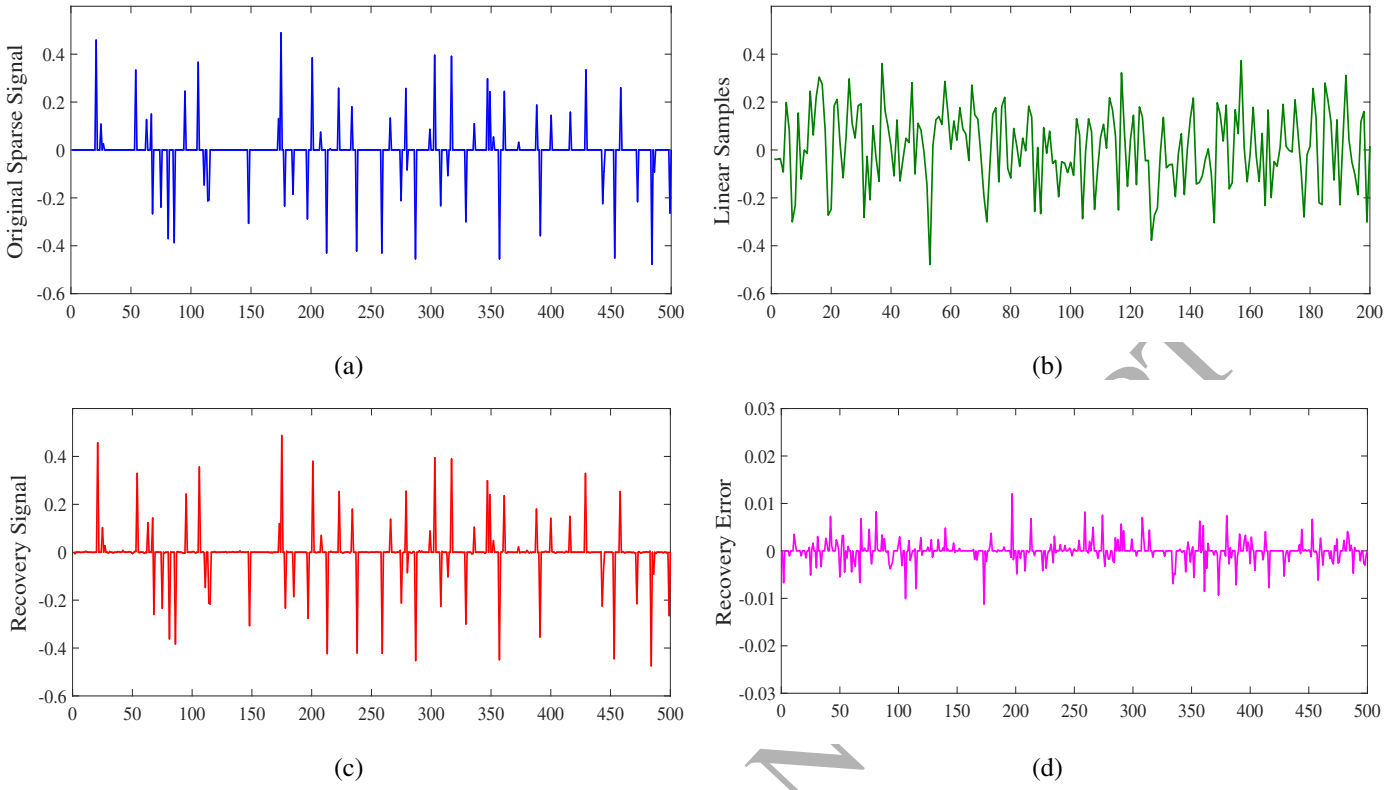

Figure 3: Performance of CSM for sparse signal: (a) original sparse signal, (b) linear samples, (c) recovery signal, (d) recovery error.

In fact, the theorem 2 can be expanded to all CSMs constructed by the i.i.d chaotic stream.

Corollary 1. For any TCcS that can generate i.i.d chaotic streams via the zone matching algorithm will construct a CSM yielding mutual coherence $u_{CSM} = \sqrt{\frac{c_4 \log(N/\gamma)}{M}}$ with the probability $Pro > 1-\gamma^2$, where $\gamma \in (0,1)$ and c_4 is a constant.

Note that the mutual coherence u_{CSM} of CSM approximates the near-optimal bound $\mathscr{O}(\sqrt{\frac{\log(N/\gamma)}{M}})$, which is similar to that of random matrices. Do *et.al* have demonstrated that the mutual coherence of Gaussian random matrix (GM) or Bernoulli random matrix (BM) is upper limited by $\mathscr{O}(\sqrt{\frac{\log(N/\gamma)}{M}})$ [15]. Moreover, if we directly use a Tent chaotic sequence generated by Eq. (4) to construct a Tent chaotic sensing matrix (TM), one can easily indicate that the mutual coherence of TM has similar boundary to that of random matrices. Obviously, $u_{CSM} \approx u_{GM} \approx u_{BM} \approx u_{TM}$, which implies that CSM has similar sampling efficiency to typical constructions.

Experimentally, we can analyze the mutual coherence of CSM by observing the entries of Gram matrix $\boldsymbol{G} \in \boldsymbol{R}^{N\times N}$ of CSM. If diagonal entries of $\boldsymbol{G}$ are approximately equal to one and off-diagonal entries of $\boldsymbol{G}$ are limited in magnitude with overwhelming probability, then the matrix is said to yield low mutual coherence. First, we construct a CSM with sizes 300×500 from the example 1 of the case 1 via the zone matching algorithm with the seed $z_1 = 0.438$ and the sampling step $d = 10$. Subsequently, the corresponding Gram matrix $\boldsymbol{G} \in \boldsymbol{R}^{500\times 500}$ shown in Fig. 2 can be easily acquired via $\boldsymbol{G} = \boldsymbol{M}_{CSM}^T \boldsymbol{M}_{CSM}$. As illustrated in Fig. 2, the majority of diagonal entries $G_{i,i}$ converge to 1 and off-diagonal entries $G_{i,j}(i \neq j)$ of $\boldsymbol{G}$ converge to 0, which implies that CSM has low mutual coherence.

3.3. Benefits of CSM

As illustrated in the above analysis, the low mutual coherence of CSM can ensure that the significant information of the signal of interest is sampled and reconstructed in CS literature. Moreover, the use of CSM for CS has the following advantages:

- Universality: The entries M_{ij} of CSM are i.i.d, which leads to the fact that the $\boldsymbol{M}_{CSM} \cdot \boldsymbol{\Psi}$ will be uncorrelated with overwhelming probability for almost all sparsifying bases $\boldsymbol{\Psi}$.
- Low complexity: If we have the initial seed z_1 and the sampling distance d of TCcS, one can rapidly regenerate CSM via the zone matching algorithm at both sampling and recovery terminals. It indicates that CSM has low complexity and low memory requirement, which would be more desired in real-time, resource-limited sampling applications.
- Hardware-friendly implementation: The CSM is a deterministic sensing matrix, which is generated from a topologically conjugate chaotic system. Becuase TCcS can be easily designed via feedback control in hardware implementation, leading to that CSM would be easily obtained in hardware.

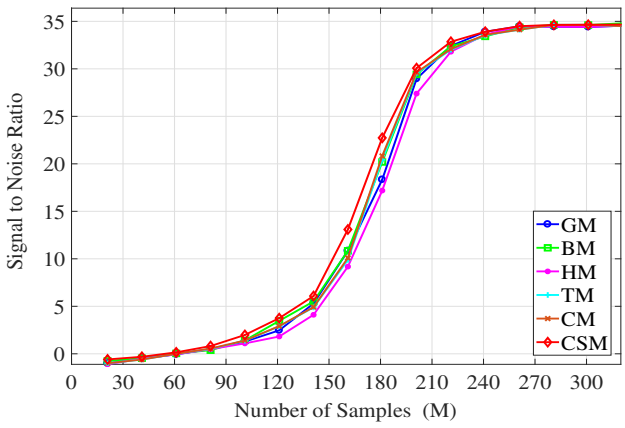

(a)

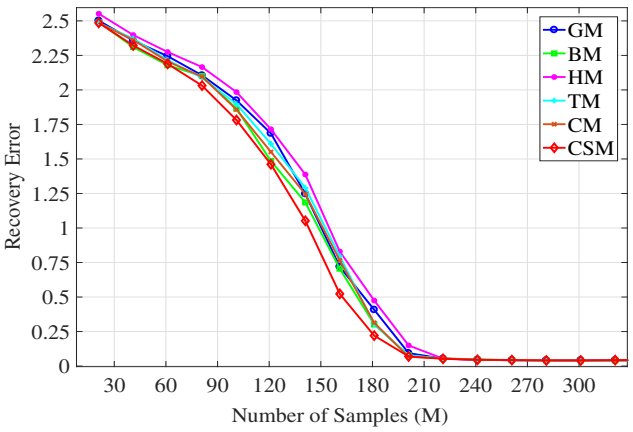

(b)

Figure 4: Performance comparisons for various sensing matrices, including GM, BM, HM, TM, CM, and CSM: (a) signal-to-noise ratios; (b) recovery errors.

- Special applications: Provided that we consider z_1 and d as the secret key to generate CSM, the CS application with CSM can be viewed as a cryptosystem in which encryption occurs implicitly at the sampling procedure. Therefore, CSM would be more favorable in particular applications, which claim privacy and security.

4. Numerical results

In this section, some numerical experiments are presented to verify the performance of CSM. For comparisons, we take the GM, BM, HM, TM, CM, and CSM for similar CS scenarios with a small amount of Gaussian noise, respectively. The GM and BM represent the Gaussian random matrix and Bernoulli random matrix [3], respectively. Both of GM and BM are conventional random sensing matrices. The full name of HM is Hadamard-Walsh matrix [16], which is a typical deterministic sensing matrix with entries 1 and -1. The TM and CM denote the Tent chaotic sensing matrix [21] and Chebyshev chaotic sensing matrix [23], respectively. Both of TM and CM are

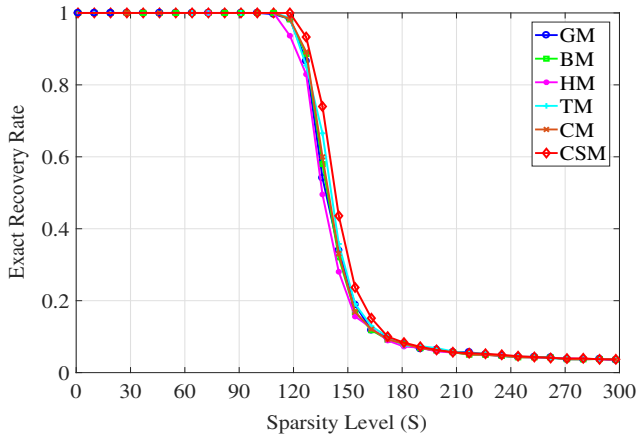

Figure 5: The exact recovery rates for different sensing matrices, including GM, BM, HM, TM, CM, and CSM.

well-performing chaotic sensing matrices based on chaotic systems. In our numerical experiments, the TM is established by Tent chaotic sequence generated by Eq. (4) with the initial value $z_1 = 0.33334$ and the sampling distance $d = 10$. The CM is built by Cheyshev chaotic sequence generated by Cheyshev system with the initial value $z_1 = 0.33334$ and the sampling distance $d = 10$. The CSM is generated from the example 1 of the case 1 via the zone matching algorithm with the seed $z_1 = 0.438$ and the sampling step $d = 10$.

4.1. CSM for sparse signal

To begin the process, we first produce a $S-$sparse, $N = 500$ length signal $\boldsymbol{x_o}$ whose elements are randomly selected from Guassian distribution $\mathcal{N}(0, 0.5)$, as drawn in Fig. 3(a).

For the chaotic CS scenario illustrated in Fig. 1, we utilize the CSM with $M = 200$ to sample such above signal with $S = 60$ at the sampling terminal, i.e., the down-sampling rate is 0.4. These linear samples $\boldsymbol{y}_o$ are sketched in Fig. 3(b). Afterwards, gaussian noise is added to simulate signal transmission through the channel, and the initial signal-to-noise ratio (SNR) is fixed at 40. At the recovery terminal, the basis pursuit denoising (BPDN) algorithm [46] is adopted to reconstruct the original signal. The recovery $\boldsymbol{x}_o^*$ and the recovery error are depicted in Fig. 3(c) and Fig. 3(d), respectively, and the corresponding SNR is 32.45. Fig. 3 shows that the sparse signal can be exactly reconstructed with a small error.

Subsequently, we make use of various sensing matrices, including GM, BM, HM, TM, CM, and CSM, to measure the original signal $\boldsymbol{x_o}$ with $S = 60$, respectively. The sampling rate is changing with the increase of the number M of the linear samples $\boldsymbol{y_o}$. The comparisons depicted in Fig. 4 are carried out by BPDN algorithm. Fig. 4(a) demonstrates the SNRs of the comparisons, and the corresponding recovery errors are drawn in Fig. 4(b).

Moreover, the aforementioned sensing matrices with same dimensions 300×500 are utilized to acquire the signal $\boldsymbol{x_o}$ with a varying sparsity level S. We define the exact recovery by $||\boldsymbol{x_o} - \boldsymbol{x_o^*}||/||\boldsymbol{x_o}|| \leq 0.3\%$ and redo each experiment 800 times.

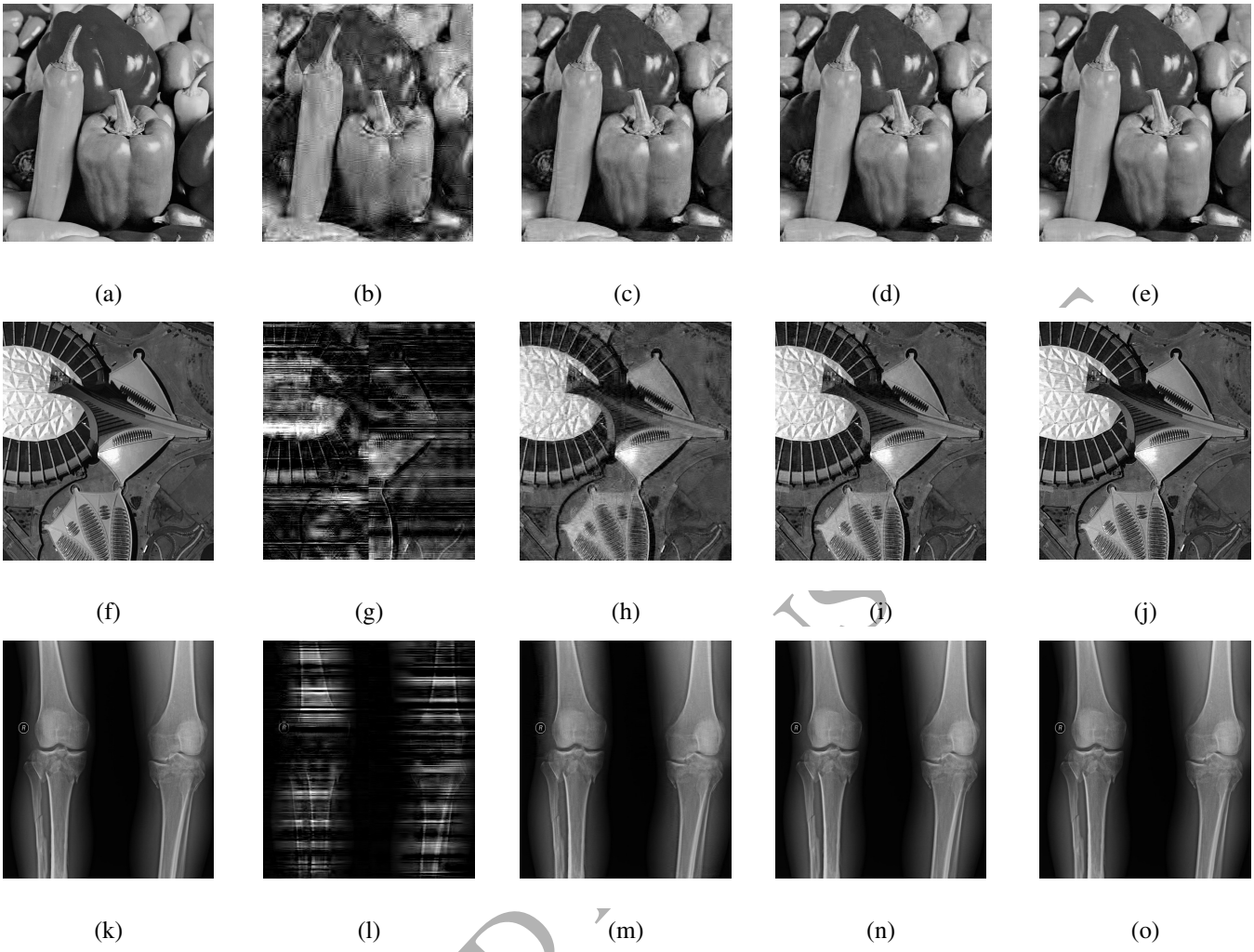

Figure 6: The original real images and the recoveries at different sampling rate: First row, natural image. (a), original "Peppers", (b) recovery with sampling rate at 0.2, PSNR=18.20; (c) recovery with sampling rate at 0.4, PSNR=27.02; (d) recovery with sampling rate at 0.6, PSNR=32.52; (e) recovery with sampling rate at 0.8, PSNR=36.27. Second row, SAR image. (f), original SAR image, (g) recovery with sampling rate at 0.2, PSNR=18.18; (h) recovery with sampling rate at 0.4, PSNR=24.48; (i) recovery with sampling rate at 0.6, PSNR=29.25; (j) recovery with sampling rate at 0.8, PSNR=34.52. Third row, medical image. (k), original medical image, (l) recovery with sampling rate at 0.2, PSNR=11.42; (m) recovery with sampling rate at 0.4, PSNR=24.58; (n) recovery with sampling rate at 0.6, PSNR=29.39; (o) recovery with sampling rate at 0.8, PSNR=32.41.

Then the exact recovery rates with respect to these matrices are compared in Fig. 5.

The results of Fig. 4 and Fig. 5 verify that CSM performs similar sampling efficiency to GM, BM, TM, and CM, but it has a slightly better sampling quality than that of HM.

4.2. CSM for image

This part demonstrates the efficacy of CSM by using image recovery from lower dimensional samples. These samples are obtained according to Eq. (1), where the $\wp$ represents Gaussian noise.

Three original signals of interest are different real images of dimensions 512×512, which are compressible in the well-designed Daubechies $9/7$ wavelet transform. Fig. 6(a) depicts a natural picture named "Peppers", Fig. 6(f) is a synthetic aperture radar (SAR) image, and Fig. 6(k) is a medical image. All of them are measured by CSM with the sampling rate at 0.2,

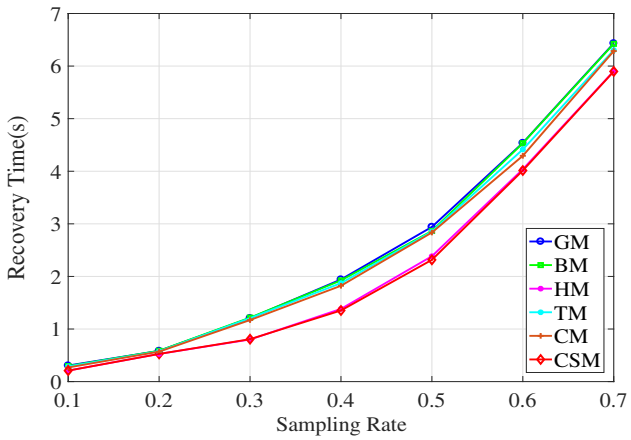

Figure 7: The recovery times of reconstructing "Peppers" for different sensing matrices at different sampling rate, including GM, BM, HM, TM, CM, and CSM.

Table 1 The competing PSNRs of image recoveries of "Peppers" with respect to various sensing matrices at different sampling rate

Sensing matrices	Sampling rate	PSNR	Sampling rate	PSNR	Sampling rate	PSNR	Sampling rate	PSNR
GM [3]	0.1	6.48	0.2	18.17	0.3	24.28	0.4	27.01
BM [3]	0.1	6.56	0.2	18.25	0.3	24.30	0.4	26.95
HM [16]	0.1	5.41	0.2	17.85	0.3	23.26	0.4	25.84
TM [21]	0.1	6.37	0.2	18.08	0.3	24.12	0.4	26.95
CM [23]	0.1	6.42	0.2	18.19	0.3	24.22	0.4	26.96
CSM	0.1	**6.49**	0.2	**18.20**	0.3	**24.33**	0.4	**27.02**
GM [3]	0.5	29.28	0.6	32.33	0.7	34.35	0.8	36.07
BM [3]	0.5	29.25	0.6	32.28	0.7	34.27	0.8	36.11
HM [16]	0.5	27.91	0.6	29.83	0.7	31.38	0.8	32.79
TM [21]	0.5	29.17	0.6	32.44	0.7	34.28	0.8	36.09
CM [23]	0.5	29.24	0.6	32.37	0.7	34.25	0.8	36.19
CSM	0.5	**29.30**	0.6	**32.52**	0.7	**34.44**	0.8	**36.27**

0.4, 0.6, 0.8, respectively. Then, we can get the reconstructions of these images by using subspace pursuit (SP) algorithm [47]. Fig. 5 presents these recoveries corresponding to different down-sampling rates. The corresponding peak-signal-to-noise ratios (PSNRs) for sub-Fig. 6(b), 6(c), 6(d), 6(e), 6(g), 6(h), 6(i), 6(j), 6(l), 6(m), 6(n), and sub-Fig. 6(o) are 18.20, 27.02, 32.52, 36.27, 18.18, 24.48, 29.25, 34.52, 11.42, 24.58, 29.39 and 32.41, separately, where the PSNR is declared by $\mathrm{PSNR}= 10\log_{10}(511\times 511)/(||\boldsymbol{x_o}-\boldsymbol{x_o^*}||^2/512/512)$.

For the purpose of comparisons, with the same CS scenario, the competing PSNRs of image recoveries of "Peppers" with respect to various sensing matrices at different sampling rate are listed in Table 1. The corresponding recovery times of reconstructing "Peppers" for these sensing matrices are shown in Fig. 7. Similarly, the PSNRs of these sensing constructions are depicted in Fig. 8(a) and Fig. 8(b), which correspond to SAR image and medical image, respectively.

As distinctly depicted in Fig. 7, the CSM can provide a slightly faster reconstruction against typical random matrices or chaotic ones. Table 1 and Fig. 8 indicate that the HM is not efficient for sampling images, including "Peppers", SAR image, and medical image. In all cases of these images, higher PSNR is obtained when the sampling rate is increased. However, there is no obvious differences in the PSNRs of these sensing matrices (including GM, BM, TM, CM, and CSM), which also implies that CSM can provide similar sampling efficiency to that of random matrices or chaotic ones. In particular, the case of "Peppers" has higher PSNR than that of SAR image or medical image. The possible reason is that SAR image or medical image is not sparse enough in the Daubechies $9/7$ wavelet transform.

In order to further explore the sampling performance of CSM, we implement five well-designed recovery algorithms to recover "Peppers" at different sampling rate. Such recovery algorithms includes the smoothed l_0 norm (SL_0), the Newton smoothed l_0 norm (NSL_0) [48], orthogonal matching pursuit (OMP), gradient projection for sparse reconstruction (GPSR), and SP algorithm. Fig. 9(a) compares the PSNRs for these recovery algorithms, and the corresponding recovery times are shown in Fig. 9(b).

From Fig. 9(a), it can be seen that, when we apply the CSM to sample the "Peppers", the SL_0, NSL_0, and SP exhibit better recovery quality than that of GPSR and OMP. Compared to other algorithms, SP performs better performance at a relatively lower sampling rate, and OMP exhibits worse recovery quality. Fig. 9(b) illustrates that the SL_0 or NSL_0 only takes a short time to reconstruct "Peppers" but OMP needs more time, which is consistent with that reported in [48]. Fig. 9 implies that CSM can be applied to CS scenarios with different recovery algorithms.

The numeral results with sparse signal or image illustrate that the proposed chaotic sensing matrices can indeed exhibit similar sampling quality for CS to that of the state-of-the-art sensing matrices. Consequently, combing with its low complexity, fast reconstruction, hardware-friendly implementation and additional encryption property, this kind of chaotic sensing matrices is strongly suggested as the sensing matrix for practical CS applications.

5. Conclusions

In this paper, we elaborate a zone matching algorithm to produce an i.i.d chaotic stream from a TCcS, which can be easily implemented via feedback control. The proposed algorithm divides one of the two transformations of the TCcS to many sub-zones according to the homeomorphism function. Then, by matching sub-zone instead of using real value of an iteration, the proposed algorithm can generate an infinite and i.i.d chaotic stream, which directly overcomes the degradation phenomenon incurred by the limited precision effects. Such an algorithm can be applied to many topologically conjugate systems, such as TCcSs of Tent chaotic system.

Therefore, by utilizing the generated i.i.d chaotic streams, we futher establish one large class of chaotic sensing matrices for compressed sensing from multiple choices of the TCcSs. Moreover, we investigate the mutual coherence of the proposed sensing matrices, and it shows that this kind of chaotic sensing matrices has comparable performance to random matrices or other chaotic constructions. Numerical results give the validations with sparse signal and real image to illustrate the com-

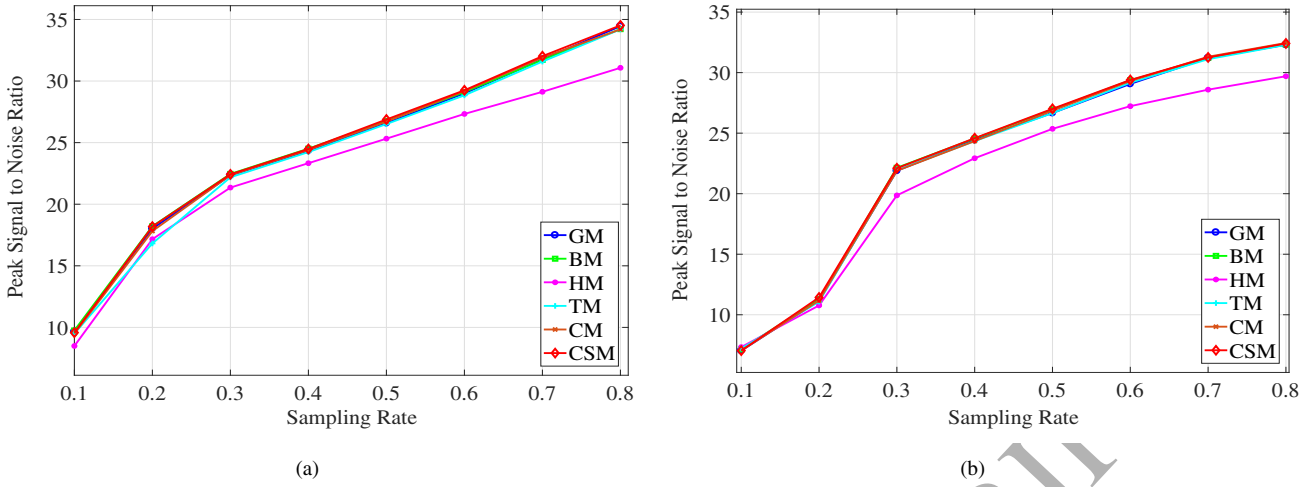

Figure 8: Performance comparisons: PSNR of image recovery versus sampling rate: (a) SAR image; (b) medical image.

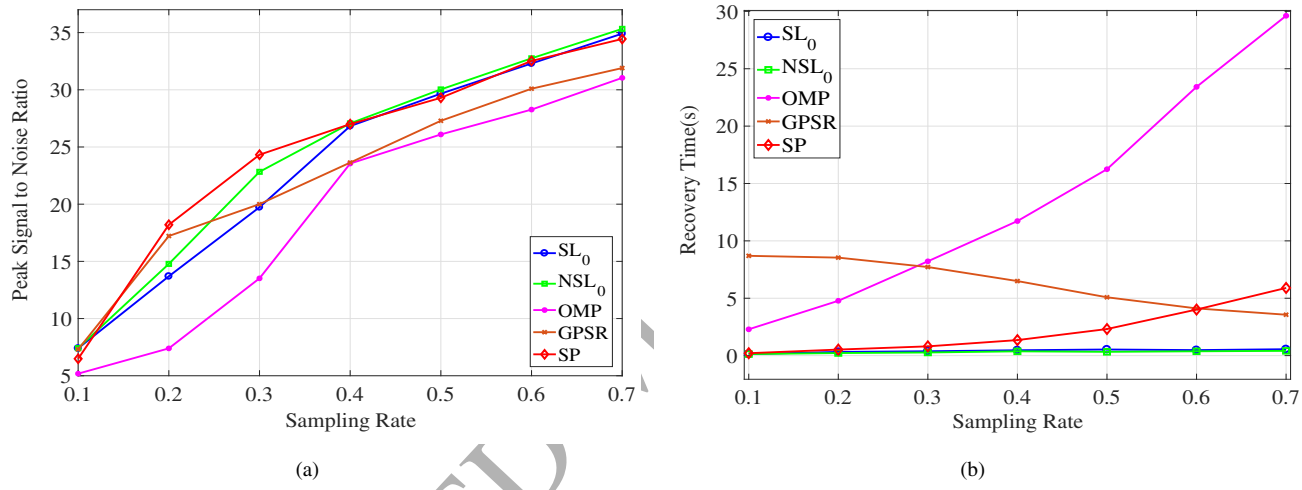

Figure 9: Performance curves for different recovery algorithms at different sampling rate: (a) peak-signal-to-noise ratios; (b) recovery times.

parability of the proposed sensing matrices to the typical ones. Compared to typical constructions, the proposed chaotic matrices have low complexity, can facilitate the hardware implementation, and would be more favorable in particular applications that claim privacy and security.

Along with the development, privacy or security and energy efficiency are significant for many applications, such as wireless body area network, healthcare monitoring system, and wireless sensor network. Thanks to the properties of CSM, compressed sensing with an our proposed sensing matrix can simultaneously solve both two key problems. Based on such a chaotic CS-based framework, the proposed sensing matrix serves as a compound operator for compressing and encrypting data within the sampling procedure, leading to that CSM supports a wide range of applications.

Although the CSM exhibits an encouraging performance, there are still many methods or algorithms trying to optimize it, such as, structuralization, QR decomposition, and sparse technique. We leave the theoretical explanation of these optimizations to our future research. Moreover, for a specific CS application with CSM, how to find a proper and efficient recovery algorithm would be a worthy topic.

Acknowledgement

This work was supported by the National Natural Science Foundation of China (NSFC No.61372069), the National Defense Pre-research Foundation, the SRF for ROCS, SEM (JY0600090102), the 111 Project of China (No.B08038), the Chongqing Municipal Education Commission (KJ1501105), the Chongqing Yongchuan Science and Technology Commission (No.Ycstc, 2015nc2001), and the Fundamental Research Funds for the Central Universities.

References

[1] P. P. Vaidyanathan, Generalizations of the sampling theorem: Seven decades after nyquist, IEEE Transactions on Circuits and Systems I: Fundamental Theory and Applications 48 (9) (2001) 1094–1109.

[2] J. Romberg, T. Tao, Exact signal reconstruction from highly incomplete frequency information, IEEE Transactions on Information Theory 52 (2) (2006) 489–509.

[3] E. J. Candès, T. Tao, Near-optimal signal recovery from random projections: Universal encoding strategies?, IEEE Transactions on Information Theory 52 (12) (2006) 5406–5425.

[4] H. Yu, J. Yang, M. Jiang, G. Wang, Supplemental analysis on compressed sensing based interior tomography, Physics in medicine and biology 54 (18) (2009) N325–N332.

[5] H. Yu, G. Cao, L. Burk, Y. Lee, J. Lu, P. Santago, O. Zhou, G. Wang, Compressive sampling based interior reconstruction for dynamic carbon nanotube micro-ct, Journal of X-ray Science and Technology 17 (4) (2009) 295–303.

[6] D. Xie, H. Peng, L. Li, Y. Yang, Semi-tensor compressed sensing, Digital Signal Processing 58 (2016) 85–92.

[7] L. Li, D. Xu, H. Peng, J. Kurths, Y. Yang, Reconstruction of complex network based on the noise via qr decomposition and compressed sensing, Scientific reports 7 (1) (2017) 15036.

[8] Y. C. Eldar, G. Kutyniok, Compressed sensing: theory and applications, Cambridge University Press, 2012.

[9] E. J. Candès, T. Tao, Decoding by linear programming, IEEE Transactions on Information Theory 51 (12) (2005) 4203–4215.

[10] E. J. Candès, The restricted isometry property and its implications for compressed sensing, Comptes Rendus Mathematique 346 (9) (2008) 589–592.

[11] J. A. Tropp, A. C. Gilbert, Signal recovery from random measurements via orthogonal matching pursuit, IEEE Transactions on Information Theory 53 (12) (2007) 4655–4666.

[12] E. J. Candès, J. Romberg, Quantitative robust uncertainty principles and optimally sparse decompositions, Foundations of Computational Mathematics 6 (2) (2006) 227–254.

[13] R. Obermeier, J. A. Martinez Lorenzo, Sensing matrix design via mutual coherence minimization for electromagnetic compressive imaging applications, IEEE Transactions on Computational Imaging 3 (2) (2017) 217–229.

[14] E. Candès, J. Romberg, Sparsity and incoherence in compressive sampling, Inverse Problems 23 (3) (2006) 969–985(17).

[15] T. T. Do, G. Lu, N. H. Nguyen, T. D. Tran, Fast and efficient compressive sensing using structurally random matrices, IEEE Transactions on Signal Processing 60 (1) (2011) 139–154.

[16] Z. Cai, H. Zhao, M. Jia, G. Wang, An improved hadamard measurement matrix based on walsh code for compressive sensing, in: Communications and Signal Processing, 2013, pp. 1–4.

[17] R. R. Naidu, C. R. Murthy, Construction of binary sensing matrices using extremal set theory, IEEE Signal Processing Letters 24 (2) (2017) 211–215.

[18] N. Li, M. Sawan, Neural signal compression using a minimum euclidean or manhattan distance cluster-based deterministic compressed sensing matrix, Biomedical Signal Processing and Control 19 (2015) 44–55.

[19] L. Yu, J. P. Barbot, G. Zheng, H. Sun, Compressive sensing with chaotic sequence, IEEE Signal Processing Letters 17 (8) (2010) 731–734.

[20] M. Frunzete, L. Yu, J. P. Barbot, A. Vlad, Compressive sensing matrix designed by tent map, for secure data transmission, in: Signal Processing Algorithms, Architectures, Arrangements, and Applications Conference Proceedings, 2011, pp. 1–6.

[21] L. Liu, P. Yang, J. Zhang, H. Ja, Compressive sensing with tent chaotic sequence, Sensors and Transducers 165 (2) (2014) 119–124.

[22] V. Kafedziski, T. Stojanovski, Compressive sampling with chaotic dynamical systems, in: Telecommunications Forum, 2012, pp. 695–698.

[23] H. Gan, Z. Li, J. Li, X. Wang, Z. Cheng, Compressive sensing using chaotic sequence based on chebyshev map, Nonlinear Dynamics 78 (4) (2014) 2429–2438.

[24] H. Gan, Z. Cheng, S. Yang, C. Liao, J. Xia, M. Lei, Circulant and toeplitz chaotic matrices in compressed sensing, Journal of Computational Information Systems 11 (4) (2015) 1231–1238.

[25] L. Zeng, X. Zhang, L. Chen, T. Cao, J. Yang, Deterministic construction of toeplitzed structurally chaotic matrix for compressed sensing, Circuits Systems and Signal Processing 34 (3) (2015) 797–813.

[26] Y. Zhang, L. Y. Zhang, J. Zhou, L. Liu, F. Chen, X. He, A review of compressive sensing in information security field, IEEE Access 4 (2016) 2507–2519.

[27] L. Y. Zhang, K. W. Wong, Y. Zhang, J. Zhou, Bi-level protected compressive sampling, IEEE Transactions on Multimedia 18 (9) (2016) 1720–1732.

[28] N. Zhou, S. Pan, S. Cheng, Z. Zhou, Image compression−encryption scheme based on hyper−chaotic system and 2d compressive sensing, Optics and Laser Technology 82 (2016) 121–133.

[29] L. Y. Zhang, K. W. Wong, Y. Zhang, Q. Lin, Joint quantization and diffusion for compressed sensing measurements of natural images, in: 2015 IEEE International Symposium on Circuits and Systems (ISCAS), IEEE, 2015, pp. 2744–2747.

[30] S. N. George, D. P. Pattathil, A novel approach for secure compressive sensing of images using multiple chaotic maps, Journal of Optics 43 (1) (2014) 1–17.

[31] L. Wan, G. Han, L. Shu, N. Feng, The critical patients localization algorithm using sparse representation for mixed signals in emergency healthcare system, IEEE Systems Journal PP (99) (2015) 1–12.

[32] C. Wang, B. Zhang, K. Ren, J. M. Roveda, Privacy-assured outsourcing of image reconstruction service in cloud, IEEE Transactions on Emerging Topics in Computing 1 (1) (2013) 166–177.

[33] J. He, G. Sun, Z. Li, Y. Zhang, Compressive data gathering with low-rank constraints for wireless sensor networks, Signal Processing 131 (2017) 73–76.

[34] H. Peng, Y. Tian, J. Kurths, Semitensor product compressive sensing for big data transmission in wireless sensor networks, Mathematical Problems in Engineering 2017 (2017) 1–8.

[35] H. Peng, Y. Tian, J. Kurths, L. Li, Y. Yang, D. Wang, Secure and energy-efficient data transmission system based on chaotic compressive sensing in body-to-body networks, IEEE Transactions on Biomedical Circuits and Systems PP (99) (2017) 1–16.

[36] S. Li, G. Chen, X. Mou, On the dynamical degradation of digital piecewise linear chaotic maps, International Journal of Bifurcation and Chaos 15 (10) (2005) 3119–3151.

[37] Q. Wang, S. Yu, C. Li, J. Lü, X. Fang, C. Guyeux, J. M. Bahi, Theoretical design and fpga-based implementation of higher-dimensional digital chaotic systems, IEEE Transactions on Circuits and Systems I: Regular Papers 63 (3) (2016) 401–412.

[38] C. Li, T. Xie, Q. Liu, G. Cheng, Cryptanalyzing image encryption using chaotic logistic map, Nonlinear Dynamics 78 (2) (2014) 1545–1551.

[39] X. F. Wang, G. Chen, Generating topologically conjugate chaotic systems via feedback control, IEEE Transactions on Circuits and Systems I: Fundamental Theory and Applications 50 (6) (2003) 812–817.

[40] Y. Deng, H. Hu, W. Xiong, N. N. Xiong, L. Liu, Analysis and design of digital chaotic systems with desirable performance via feedback control, IEEE Transactions on Systems, Man, and Cybernetics: Systems 45 (8) (2015) 1187–1200.

[41] Z. G. Xu, Q. Tian, L. Tian, Theorem to generate independently and uniformly distributed chaotic key stream via topologically conjugated maps of tent map, Mathematical Problems in Engineering 2012 (2012) (2012) 1695–1698.

[42] T. Kohda, Information sources using chaotic dynamics, Proceedings of the IEEE 90 (5) (2002) 641–661.

[43] I. Bhaumik, B. Choudhury, Topologically conjugate maps and ω-chaos in symbol space, International Journal of Applied Mathematics 23 (2) (2010) 309–321.

[44] P. Glendinning, Topological conjugation of lorenz maps by $\beta-$transformations, Mathematical Proceedings of the Cambridge Philosophical Society 107 (2) (1990) 401–413.

[45] B. L. Hao, Starting with parabolas: an introduction to chaotic dynamics, Shanghai Scientific and Technological Education Publishing House, 1993.

[46] W. Lu, N. Vaswani, Regularized modified bpdn for noisy sparse reconstruction with partial erroneous support and signal value knowledge, IEEE Transactions on Signal Processing 60 (1) (2012) 182–196.

[47] D. Wei, O. Milenkovic, Subspace pursuit for compressive sensing signal reconstruction, IEEE Transactions on Information Theory 55 (5) (2009) 2230–2249.

[48] M. M. Hyder, K. Mahata, An improved smoothed approximation l_0 algorithm for sparse representation, IEEE Transactions on Signal Processing 58 (4) (2010) 2194–2205.